BeBeC-2022-D11

DIPOLAR-BASED EQUIVALENT SOURCES METHOD FOR THREE-DIMENSIONAL AEROACOUSTIC SOURCE IDENTIFICATION

Joannès Chambon[1,2], Olivier Minck[1], Simon Bouley[1], and Jérôme Antoni[2]
[1]MicrodB
28 Chemin du Petit Bois, F-69134, Écully, France.
[2]Univ Lyon, INSA Lyon,
Laboratoire Vibration et Acoustique, 25 bis av. Jean Capelle, F-69621, Villeurbanne, France.

Abstract

In accordance with aeroacoustic analogies, the noise arising from the interaction of an object and a low Mach number flow is likely to be accurately described by the radiation of elementary monopoles, dipoles and quadrupoles. Combined with the diffracting behaviour of the car as a rigid body, three-dimensional source identification in wind tunnel is thus prone to sketchy or misleading interpretations when only free field monopolar steering vectors are used.

With a view to provide relevant beamforming maps for 3D acoustic imaging, this paper investigates model refinements inspired from aeroacoustic analogies. In this framework, it is assumed that loading noise dipoles prevail over cavities and vortices produced acoustic sources. A variation of the Equivalent Source Method is proposed to account for the scattered part of the acoustic transfer toward the microphone array. This approach is derived to deal with dipolar source identification and assessed analytically on an academical test case.

Finally, the choice is made to present industrial results from Computational Fluid Dynamic based simulated acoustic fields. The latter are becoming widespread to design car pieces upstream to actual wind tunnel measurements since they enable to put source models to the test without struggling with installation effects. The identification of sound sources produced by a flow impinging an Idealized Side Mirror is discussed, in light of the proposed Equivalent Source Method presented in the first sections.

Introduction

As an inverse problem, sound source localisation in three dimensions relies on two distinct cornerstones. One is the physical model chosen to describe the acoustic propagation of the sources to identify and the other is the algorithmic process used to derive information from measured acoustic data. The second aspect accounts for an important part of the acoustic imaging literature, and a wide scope of algorithms have been assessed depending on the assumption made on the acoustic sources (see Merino-Martinez *et al.*, 2019; Leclère *et al.*, 2017). The first however is a less investigated lead for improvement, mainly because alternatives to analytic transfer functions are often either numerically demanding (Boundary Element Method, Finite Element Method) or impractical (measured transfer functions, see Holland and Nelson, 2012). For that purpose, the Equivalent Source Method developed by Koopmann *et al.* (1989) has been put forth and assessed as a powerful tool by Le Magueresse (2016) to simulate monopolar propagation models accounting for scattering object in the acoustic scene.

When it comes to aeroacoustic imaging, another potential improvement can be the directivity of the investigated sources. The first section of this paper is a short overview of the aeroacoustic analogies involved in noise production at low Mach numbers. It emphases the fact that dipolar directivity patterns are likely to be more relevant to identify noise produced by a rigid body inside a flow.

Then section 2 proposes an Equivalent Source Method aiming at the simulation of dipolar acoustic transfer functions. This new approach is presented as a complementary development of the ESM as used by Chambon *et al.* (2020) for acoustic imaging in wind tunnel.

Finally, the last part consists in the presentation of Idealized Side Mirror case on which various propagation models are benchmarked. Both free-field and ESM transfer functions are put to the test with a virtual microphonic pressures stemming from a CFD computation.

1 3D imaging on CFD issued data

Given the complexity of the hydrodynamic phenomena responsible for noise production, a large field of aeroacoustic research leads is dedicated to the refinement of acoustic analogies. Using integral methods, such a formalism allows to compute the far field propagation of aerodynamically produced noise given the knowledge of the local flow properties.

Ffowcs Williams and Hawkings (FW-H) source terms

From the introduction of aeroacoustic analogies by Lighthill (1952) to the current state of the art, a wide range of source terms interpretations were established with regard to the hypotheses made on the test case.

Considering the set up of wind tunnel measurements, i.e. sound received by stationary observers from the interaction of a flow and a rigid structure, a redraft of Lighthill's equations were proposed first by Curle (1955) and buttressed by Ffowcs Williams and Hawkings (1969).

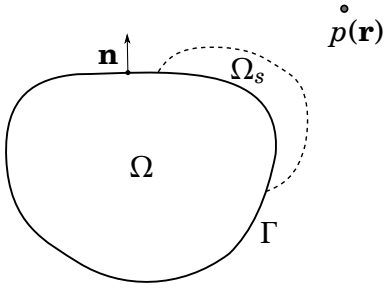

Fig. 1 - *FW-H schematic set up.* Ω *and* Γ *denote the interior and the boundary of the structure, while* Ω_s *accounts for the source area. The pressure at the observer point* $\mathbf{r}$ *can be obtained from the source region only.*

The generic formulation of FW-H analogy in the spectral domain (See Casalino, 2002, p.422) is given by

$$\begin{aligned} p(\mathbf{r},\omega) = &-\int_{\Omega_s} T_{ij}\frac{\partial^2 G(\mathbf{r}|\mathbf{r}_s,\omega)}{\partial x_i \partial x_j}\mathrm{d}\mathbf{r_s} \\ &+\int_{\Gamma} L_i \frac{\partial G(\mathbf{r}|\mathbf{r}_s,\omega)}{\partial x_i}\mathrm{d}\Gamma(\mathbf{r_s}) \\ &-\int_{\Gamma} \mathrm{i}\omega Q G(\mathbf{r}|\mathbf{r}_s,\omega)\mathrm{d}\Gamma(\mathbf{r_s}), \end{aligned} \tag{1}$$

where the G function is the free field Green function.

The three source terms on the right-hand of Eq. (1) are respectively defined as :

- Lighthill's tensor T_{ij} : associated to the quadrupolar radiation pattern, it accounts for the self-induced turbulence component in the source volume.
- The surfacic dipolar sources L_i, often referred to as *loading noise*, transcribing the pressure changes due to the body reactive forces interacting with the flow.
- The surfacic monopolar sources Q, sometimes named *thickness noise*, stemming from mass of fluid moved by a the body surface.

Straightforward interpretations of the three source terms as proposed on Fig-2 may be untrue for some specific set ups. This source description is to be understood as a guideline more than a actual set in stone definition (see Norton and Karczub, 2003, section 2.4.3, for a summarized rendering of FW-H analogy).

The commonly used process to benefit from this formulation is to numerically compute the physical properties of the flow inside Ω_s (pressure, particle velocity, density) thanks to an incompressible simulation tool (for instance a Large Eddy Simulation (LES) model) to get the acoustic pressure at any observer location outside the source region thanks to FW-H integrals.

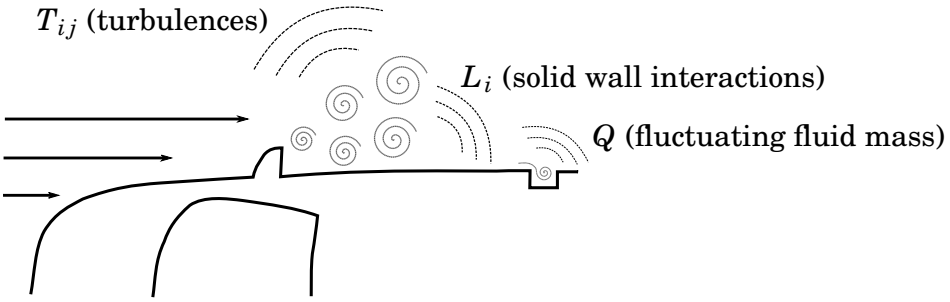

Fig. 2 - *Source terms in FW-H analogy exemplified on a car (inspired by Blumrich and Helfer, 2017).*

Formulation for wind tunnel applications

The classic FW-H formulation covers a wide range of applications as long as it addresses the noise produced by any moving body inside a medium at rest. As the emphasis of this paper is put on source identification from wind tunnel measurements, some hypotheses can be considered to reduce the complexity of the source models.

First of all, it appears that the orders of magnitude of noise resulting from each source type can be related to the Mach number M_0 of the flow. This commonly used result (see Norton and Karczub, 2003, section 2.4.3, for a brief justification) states that in terms of acoustic intensity I

$$I_Q \sim M_0, \quad I_L \sim M_0^3, \quad I_T \sim M_0^5 \tag{2}$$

where M_0 is the mach number.

Bearing in mind that wind speed in automotive wind tunnel hardly exceeds $M = 0.1$, quadrupolar sources related to the turbulent flow-induced noise are often neglected. Some other simplifications can be provided to Q and L_i.

The last step to fall in the scope of wind tunnel testing and get a specific view point of FW-H analogy is to consider a convected wave equation when computing the Green function since FW-H sources are to be propagated in a moving medium. It was formulated and refined by Najafi-Yazdi *et al.* (2011). Ultimately, the optimized formulation referred to as *1C* in the literature reads as follows in the frequency domain while neglecting quadrupoles (with the notation of Fig-1) :

$$p(\mathbf{r}) = \int_\Gamma L_i \left[\mathrm{i}k\tilde{R}_i + \frac{\tilde{R}_i^*}{R^*} \right] \frac{\mathrm{e}^{\mathrm{i}kR}}{4\pi R^*} \mathrm{d}\Gamma(\mathbf{r}_s) - \mathrm{i}\omega \int_\Gamma Q \frac{\mathrm{e}^{\mathrm{i}kR}}{4\pi R^*} \mathrm{d}\Gamma(\mathbf{r}_s), \tag{3}$$

where

$$\begin{aligned} &\delta\mathbf{r} = \mathbf{r}_s - \mathbf{r}, \quad \delta r = \|\delta\mathbf{r}\|, \quad \beta^2 = \left(1 - M_0^2\right), \\ &R = \frac{1}{\beta^2}\left(R^* - \mathbf{M}_0 \cdot \delta\mathbf{r}\right), \quad \text{and } R^* = \delta r \beta \sqrt{1 + \beta^2 \mathbf{M}_0 \cdot \delta\mathbf{r}}. \end{aligned} \tag{4}$$

Loading noise in acoustic imaging

Regarding the previous paragraphs, it is relevant to draw a distinction between monopolar and dipolar propagation models. Such a separation in acoustic imaging lies in the choice of the steering vectors supplied to beamforming, or more generally in the construction of the Frequency Response Function (FRF) $\mathbf{H}$ chosen for the classical inverse problem formulation

$$\mathbf{p} = \mathbf{H}\mathbf{q} \tag{5}$$

between pressures $\mathbf{p}$ sensed by a microphone array and source $\mathbf{q}$ on discretized mesh of a radiating object.

The monopolar pattern is the historical and the most commonly used transfer function. It got extensively studied as a steering vector (see Sarradj, 2012; Chardon, 2022) and proved out to be a robust approach in the general case.

However, it is not the most physically relevant for loading noise identification. Because of the monopole lack of directivity, monopole based beamforming maps can be misleading and overestimate sources perpendicular to planar arrays. For that reason, Jordan *et al.* (2002); Liu *et al.* (2008) first investigated the introduction of free-field dipolar transfer function in beamforming. More recently, Porteous *et al.* (2015) and Gao *et al.* (2020) extended this approach to 3D source identification. On the basis of these articles, it appears that dipolar FRFs lead to insightful imaging maps for the characterization of aeroacoustic sources based on array measurements.

2 Dipolar Equivalent Source Method

Three-dimensional imaging of acoustic sources related to scattering structures is a recently tackled issue. For the specific case of loading noise issued from a flow impinging a body, Evans *et al.* (2019) designed a *half dipole* formulation to filter the dipole directivity that would propagated through the scattering body. This approximation stands as a simple and robust approach to include the rigid behaviour of the body in the propagation model, but other numerical methods were recently exposed in the literature for the same purpose.

ESM for FRF construction

Using the reciprocity principle, Chambon *et al.* (2020) and Le Magueresse *et al.* (2020) designed an Equivalent Source Method (ESM) computing monopolar FRFs for acoustic imaging that includes three-dimensional scattering effects. ESM was assessed on analytical and experimental wind tunnel data with planar arrays. It shown interesting improvements both in terms of resolution and source localization when applied to beamforming, but at the cost of large computational resources and additional user-defined adjustment parameters. In a nutshell, ESM consists in tuning a set of monopoles inside the scattering object with regard to the reflection boundary condition imposed on its skin. Then these sources are backpropagated toward the array given an incident field depending on the microphone position (see Chambon *et al.*, 2020, for the complete depiction of the process).

In the continuation of this work, the aim of this paper is to propose a linkage between the dipolar source model associated to loading noise and the ESM. Such an approach leads to the simulation of dipolar FRFs that take into account diffracting surfaces in the acoustic scene.

Description of the method

The statement of the problem reads exactly as follows : a rigid body placed in a uniformly moving medium is modelled by N nodes composing a mesh. A distribution of dipolar sources of complex amplitudes $\mathbf{q} \in \mathbb{C}^N$ is to be recovered, on the basis of M measured pressure $\mathbf{p} \in \mathbb{C}^M$ and a propagation model $\mathbf{H} \in \mathbb{C}^{N\times M}$. A basic illustration of the geometrical set-up is displayed on Fig-3.

The emphasis of this article is put on the construction of the propagation model. As mentioned above, Evans *et al.* (2019) proposed a straightforward free-field formulation as

$$\mathbf{H}_{ij} = \mathbf{D}_{ij} = \begin{cases} A_j \frac{\mathrm{e}^{\mathrm{i}kr_{ij}}}{4\pi r_{ij}^2}(1-\mathrm{i}kr_{ij})\,\mathbf{r}_{ij}\cdot\mathbf{n}_j & \text{if} \quad \mathbf{r}_{ij}\cdot\mathbf{n}_j > 0 \\ 0 & \text{if} \quad \mathbf{r}_{ij}\cdot\mathbf{n}_j < 0, \end{cases} \tag{6}$$

where $\mathbf{r}_{ij} = \mathbf{r}_j - \mathbf{r}_i$ and $r_{ij} = \|\mathbf{r}_{ij}\|$. A_j denotes the surface of the j^{th} element of the mesh. Here the condition related to the incident angle serves as a filter to remove microphones located in the blind spot of the dipole : without it, any small coherent signal leads to largely overestimated sources because of the steering vector tending toward zero.

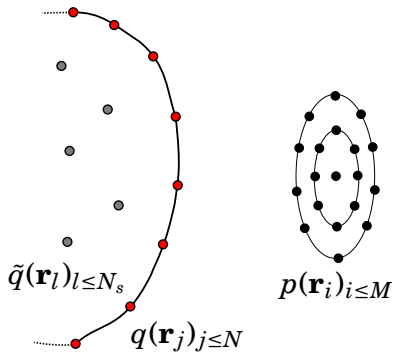

Fig. 3 - *Schematic set up for FRFs simulation based on ESM. The grey dots are equivalent monopolar sources used to ensure a zero normal velocity on the mesh.*

ESM takes the form of an intermediary step in the computation of $\mathbf{H}_{ij}$. Given a grid point $\mathbf{r}_j$ and a microphone $\mathbf{r}_i$, its process is described below :

1. Calculation of the normal velocity radiated by a dipole on $\mathbf{r}_i$ oriented by $\mathbf{n}_j$ (see Fig-4 for an illustration) on every node of the mesh. This quantity is the incident velocity that equivalent sources will offset and stems from the derivation of Eq. (6) :

$$\forall \alpha \leq N, \quad \mathbf{v}_\alpha^{ij} = A_j \frac{\mathrm{e}^{\mathrm{i}kr_{i\alpha}}}{4\pi r_{i\alpha}^3} \begin{bmatrix} \left(k^2 r_{i\alpha}^2 - 2\mathrm{i}kr_{i\alpha} + 2\right)\mathbf{r}_{ij}\cdot\mathbf{n}_j \\ \mathrm{i}kr_{i\alpha} + 1 \end{bmatrix} \cdot \mathbf{n}_\alpha. \tag{7}$$

2. Calibration of the equivalent monopoles inside the object ($\tilde{\mathbf{q}}$ on Fig-3) through

$$\tilde{\mathbf{q}}^{ij} = \nabla\mathbf{G}^{+}\mathbf{v}^{ij}, \tag{8}$$

where $\nabla\mathbf{G} \in \mathbb{C}^{N\times N_s}$ is filled with the free-field normal velocity of the equivalent sources toward the mesh. The + superscript denotes the pseudo-inversion.

3. Final back propagation of both the incident dipolar pressure field and the equivalent scattered pressure on the node of interest :

$$\mathbf{H}_{ij} = \underbrace{\mathbf{D}_{ij}}_{\text{incident}} + \underbrace{\mathbf{G}\tilde{\mathbf{q}}^{ij}}_{\text{scattered}}, \tag{9}$$

$\mathbf{G} \in \mathbb{C}^{N\times N_s}$ being the free-field pressure propagator of the equivalent sources.

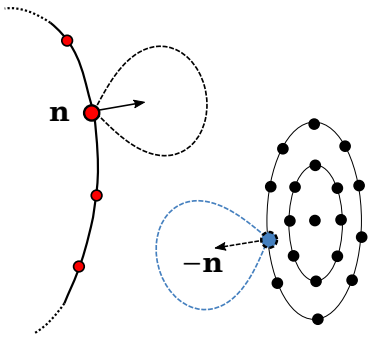

Fig. 4 - *Reciprocity principle applied to dipolar FRFs. The computation of a half dipole on the mesh radiating toward a microphone can be traded against the one of a dipole with opposite direction located on the array toward the surface.*

All in all, this methodology provides the FRF between a dipole on the position of the i^{th} microphone toward the j^{th} node of the mesh. After iterating it for all $i \leq M$, $j \leq N$, the reciprocity principle states that the Hermitian conjugate of the obtained $\mathbf{H}$ matrix equals the transfer function between dipoles on the mesh and the array.

The concerns about numerical stability of ESM are almost the same as those exposed by Chambon *et al.* (2020) (see also Lee, 2017, for a more in-depth sensitivity review). There are still some notable differences with the monopole ESM version :

- The computational cost is increased. The costliest steps from that perspective are the pseudo inversion of $\nabla\mathbf{G}$ ($\mathcal{O}(N_s N^2)$ operations) and the loop on every node on the mesh to compute the incident velocity vector. The first represents the same challenge as with the classical version of ESM, but the second is more demanding with dipoles because of the j dependency in Eq. (7) (which cannot be vectorized). The overall cost remains in $\mathcal{O}(N_s N^2)$, but dipolar ESM features double the number of operations as before.

- A greater care has to be taken regarding the quality of the mesh. Poorly defined normal vector values and direction leads to inaccurate values of normal velocity $\mathbf{v}^{ij}$. Since $\nabla\mathbf{G}$ is often ill-conditioned, it is of importance to keep an adequacy on the node normals in order not to rely too much on regularization to solve Eq. (8).

3 Sound source identification : Idealised Side Mirror

Once tackled the problematic of the propagation model, identification of aeroacoustic sources remains prone to a wide range of additional issues : ground and wall reflections, shear layer decorrelation, flow-induced noise, etc. A relevant alternative to testing is the production of signals based on Computational Fluid Dynamic (CFD).

Model description

The test case is an Idealized Side Mirror (ISM). It consists in an half cylinder topped with a quarter sphere. This model is already partly studied in the literature, Wang *et al.* (2010) firstly investigated this geometry and achieved to propagate the far field pressure at $M_0 = 0.11$ using LES and a Boundary Element Method (BEM). More recently, Pan *et al.* (2020) did the same and shown interesting radiated pressure maps supplied to a vibroacoustic software.

The ISM under scrutiny here is displayed on Fig-5. It notably features three small design flaws on its side and its top to trigger interactions with the flow and be closer to a genuine side mirror. The corresponding mesh features $N = 5506$ nodes for a characteristic length L equal to 0.3 meters.

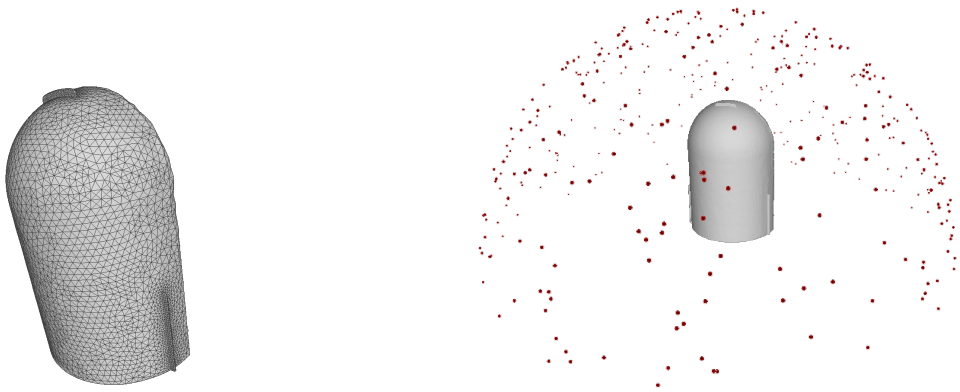

(a) **(b)**

Fig. 5 - *Idealized Side Mirror geometry. (a) Triangular mesh of the modified ISM with top and side flaws. (b) Simulated microphone positions for CFD computation.*

The microphone array is a cloud of $M = 400$ points randomly distributed on a hemisphere of radius $a = \frac{5}{3}L$ fully covering the ISM. Its geometry is not particularly optimised, but the high number of microphones yields good performances in terms of sidelobes as

exposed on Fig-6. On this figure are displayed the free-field Point Spread Function (PSF) on a plane centered on the barycentre of the ISM.

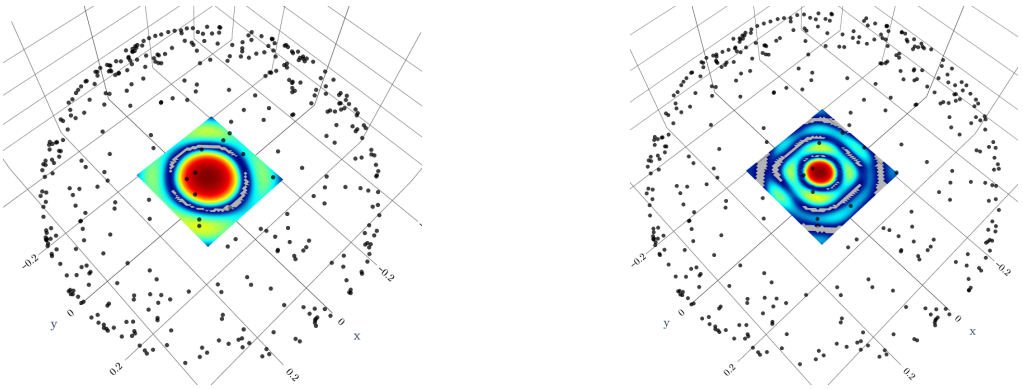

(a) **(b)**

Fig. 6 - *Point Spread Function of the ISM array geometry (24 dB dynamic range); (a)* $f = 1500$ *Hz; (b)* $f = 3000$ *Hz.*

Regarding ESM, the parameters chosen for the FRF computation are chosen in accordance with empirical statements made by Dunn and Tinetti (2004) : the number of equivalent sources is set to a third of the amount of control points ($N_s = \frac{1}{3}N = 1830$), and their spatial distribution is a 80% scaled replica of the mesh.

CFD data

The temporal signals associated to each microphone is computed using the Acoustic Perturbation Equation (APE) available in Siemens (Siemens 2021) software Star CCM+. The latter is finite difference approach designed by Ewert and Schröder (2003) that allows to predict the acoustic perturbations related to the ISM geometry and propagate them directly toward the array.

The CFD outputs take the form of 0.3 seconds time signals sampled at $f_s = 25$kHz. For the Cross Spectral Matrices (CSM) computation, a Welch periodogram is used with a Hann window and a 50% overlap between snapshots. As exposed on Fig-7 and in adequation with the results obtained by Pan *et al.* (2020), no particular frequency emerges from the ISM geometry in terms of acoustic radiation.

On Fig-8 can be observed the pressure levels from the APE simulation in the frequency domain. The trend seems to be that the low frequency component of the signal corresponds to extended source distribution on the mesh with maximum levels downstream, while at higher frequency the energy gets concentrated on the small flaws impinged by the flow (and in particularly the top one).

Beamforming maps

Chambon *et al.* (2020) pointed out that conventional beamforming was an uncertain approach when not using non free-field monopole propagators. Indeed, the $\frac{1}{\|\cdot\|^4}$ denominator makes it prone to numerical instability when steering vectors take small or null

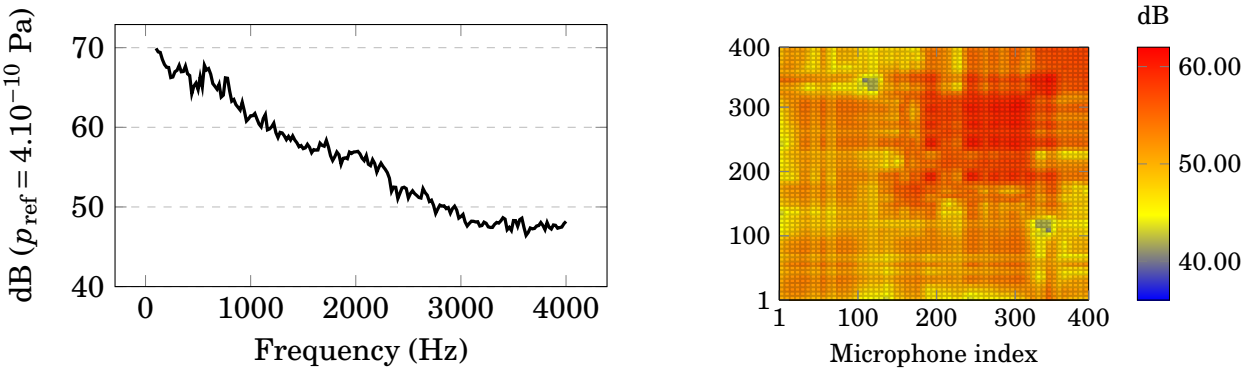

(a) **(b)**

Fig. 7 - *CFD issued spectra on the array for the ISM at $M_0 = 0.11$; (a) average autospectra on the 400 microphones; (b) CSM at $f = 1500$ Hz.*

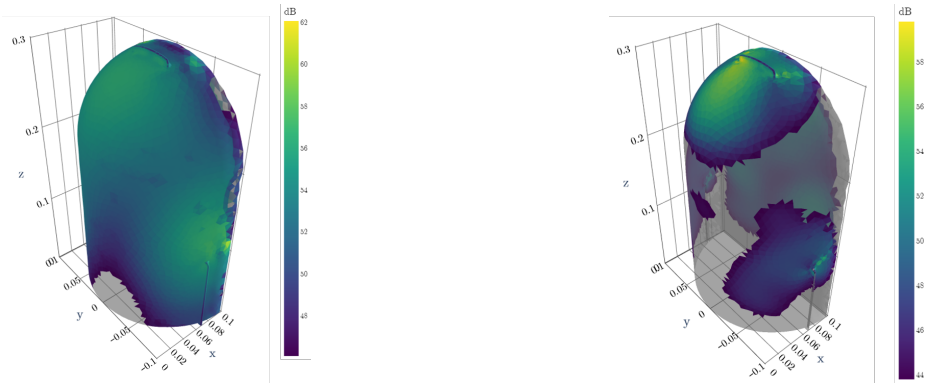

(a) **(b)**

Fig. 8 - *Element-wise surface pressure PSD on the ISM at $M_0 = 0.11$ (a) $f = 1000$ Hz; (b) $f = 3000$ Hz. 16 dB dynamic range.*

values, which can be the case with ESM based or directive transfer functions. Similarly to what was proposed by Leclère *et al.* (2020), a Coherence Beamforming is thus chosen. Noting $\mathbf{S_{pp}}$ the CSM of the microphones and keeping the notations of section 2, sources are estimated by

$$\left|q\left(\mathbf{r}_j\right)\right|^2 = \frac{\mathbf{H}_j \mathbf{S_{pp}} \mathbf{H}_j^{\mathsf{H}}}{\left\|\mathbf{H}_j\right\|^2 \mathrm{Tr}\left(\mathbf{S_{pp}}\right)}, \; j \leq N. \tag{10}$$

This variation of beamforming is an unquantified indicator that allows to seize the correlation between the simulated pressures on the array and the potential source on the j^{th} point of the mesh. At that stage, it should be precised that no denoising algorithm is applied to the CSM since it stems from a noise-free simulation. This is furthermore noticeable on Fig-7 (b) where the diagonal does not emerge in comparison to interspectra. Notably, the commonly used diagonal removal technique is irrelevant here because of the non zero trace in Eq. (10).

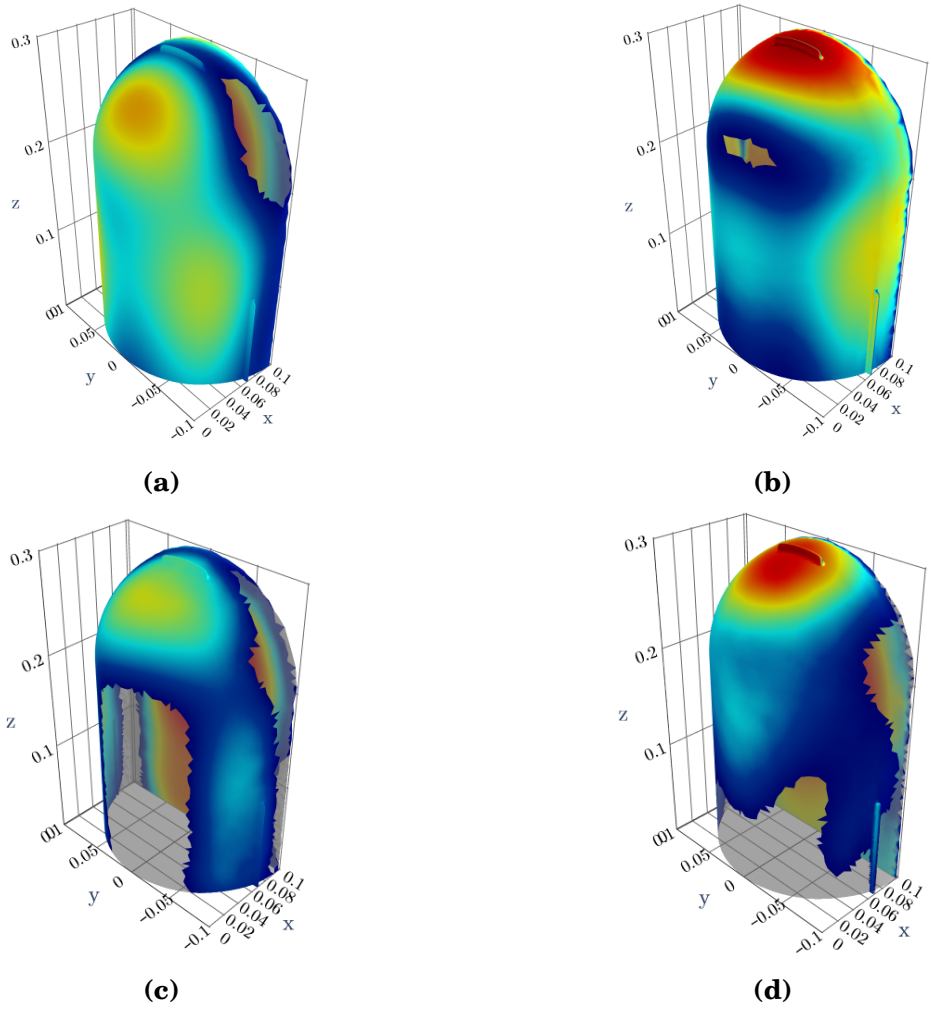

Fig. 9 - *Coherence beamforming maps at f = 1500 Hz, 12 dB dynamic range. (a) Free-field monopolar FRF; (b) free-field dipolar FRF; (c) ESM FRF; (d) dipolar ESM FRF.*

From Fig-9 it can be inferred that all four models yield to slightly different interpretations. According to the monopolar output maps on the left, noise sources are not specifically related to the presence of the flaws in contradiction with the results on the right that features the directive source model. In both case, the intermediate use of ESM can be associated to a resolution improvement. A common ground is the main lobe located on the rear face of the mirror, which is consistent with the results of Pan *et al.* (2020) where most of the energy is concentrated downstream.

At a higher frequency on Fig-10 the conclusions differ : both monopole approaches indicate that the sources are located upstream to the additional flaws. Having in mind the surface pressure exposed in Fig-8 (b), such a conclusion is decent but misses the actual fine pressure maxima located on the edge of the top and side flaws. From that perspective, dipolar models could offer a complementary interpretation but it appears

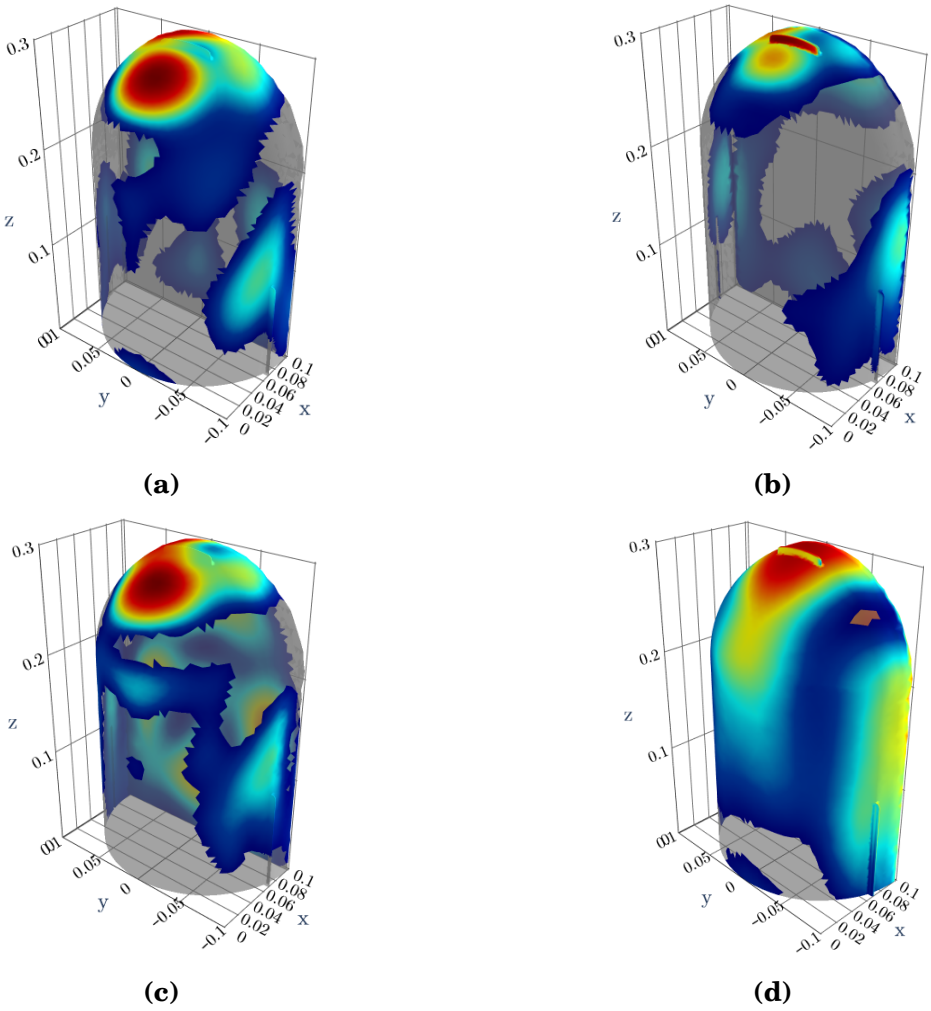

Fig. 10 - *Coherence beamforming maps at 3000Hz, 12 dB dynamic range. (a) Free-field monopolar FRF; (b) free-field dipolar FRF; (c) ESM FRF; (d) dipolar ESM FRF.*

that beamforming poorly handles directive FRFs in that case. The irregularity on the top flaw in Fig-10 (d) is a insightful example : considering grid points on the rear side of the flaw, its acoustic transfer with the front microphones is not taken into account because of the half dipole directivity, while the transfer with the rear part of the array is weak because of the masking effect of the ISM body. An illustrative result of this phenomenon is displayed on Fig-11.

Inverse method

A solution to avoid the hazardous relationship between beamforming and singular steering vector is to switch to a inverse method that inverts the full **H** matrix. This is achieved here through the application of iterative Bayesian Focusing, an inverse method designed by Antoni (2012). Its practical implementation is depicted by Le Magueresse *et al.* (2020, section 3.1). Following the guidelines of this reference, the regularization pa-

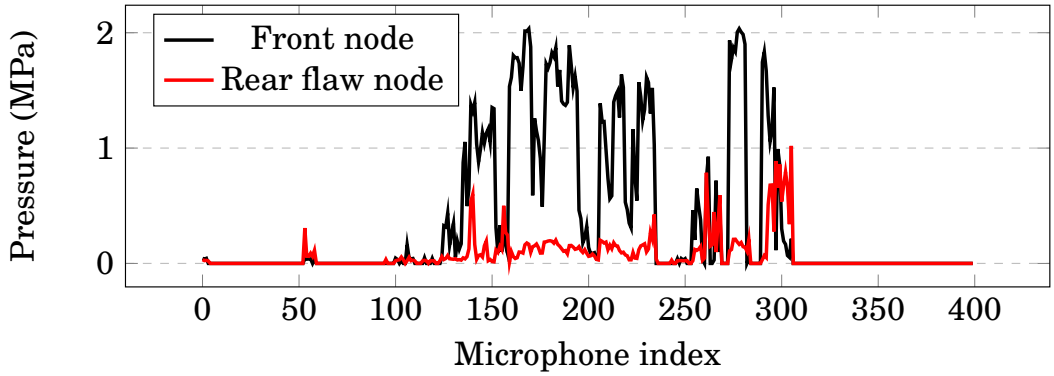

Fig. 11 - *FRF amplitude between two specific nodes and the 400 microphones at* $f = 3000$ *Hz.*

rameter of Bayesian Focusing is set to the default value $p = 1.3$ while the initial spatial aperture is chosen uniform.

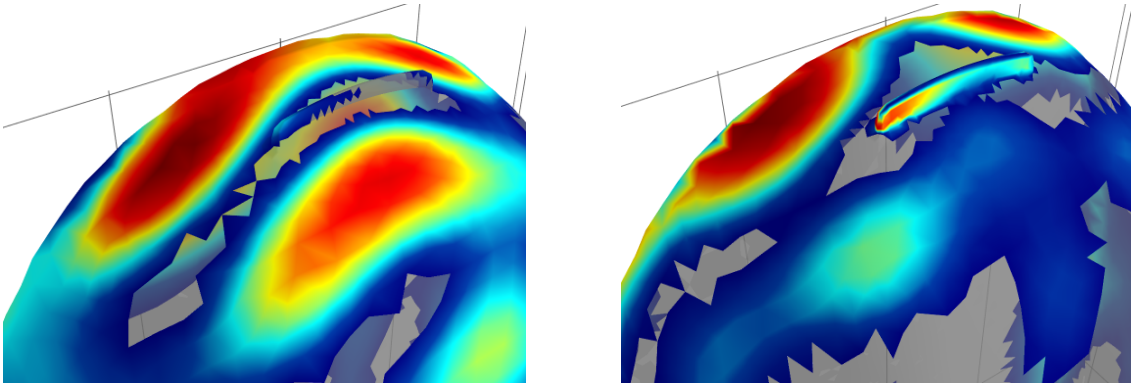

(a) **(b)**

Fig. 12 - *Iterative Bayesian Focusing maps at 3000 Hz, restrained to the top part of the ISM with a 20 dB dynamic range. (a) ESM FRF; (b) dipolar ESM FRF.*

The result is plotted on Fig-12. The most convincing set-up to have a proper depiction of the detailed sources around the tips of the top flaw on the ISM is the combination of iterative Bayesian Focusing and dipole ESM transfer functions.

Conclusion

With a view to supply acoustic imaging algorithms with more realistic propagation models, a link with the aeroacoustic analogy literature is discussed. In the context of aeroacoustic source reconstruction, dipoles are included in the ESM process so that 4 models could be used : monopoles or dipoles distribution on the skin of a rigid body inside a flow, with or without the coverage of scattering effects.

The application of these approaches on the case of an ISM with aerodynamic flaws reveals that both monopoles and dipoles provide relevant and complementary insights on the surface pressure. The greater degree of precision on high frequency pressure reconstruction is achieved when a dipolar ESM model is provided to an inverse method. It was also shown that a specific care should be taken when using beamforming for 3D acoustic imaging with directive transfer functions.

Avenues for further enhancements are numerous : an in-depth study on a mixed monopole/dipole approach would be physically suitable and the current process using one model at a time probably remains erroneous. It may also be interesting to benchmark propagation models on more complex geometries to have a clearer view on their relevance.

Acknowledgements

Authors would like to thank Mr.Hironori Tokuno and Mr.Alexander Schell from Daimler for the Star-CCM+ computation and the insightful discussions on the ISM test case.

This work was partially performed in the framework of the CALM-AA project, funded by Région Auvergne Rhône-Alpes (AURA), BPI France and the European Union through the European Regional Fund (FEDER).

References

Antoni, J. (**2012**). "A Bayesian approach to sound source reconstruction : Optimal basis, regularization, and focusing," Journal of the Acoustical Society of America **131**, 2873–2890, doi: 10.1121/1.3685484.

Blumrich, R., and Helfer, M. (**2017**). "Application of wind tunnels for automotive aeroacoustic development," Science an Technology Organization .

Casalino, D. (**2002**). "Analytical and numerical methods in vortex-body aeroacoustics," Ph.D. thesis, thèse de doctorat dirigée par Roger, Michel et Chiocchia, Gianfranco Acoustique Ecully, Ecole centrale de Lyon 2002.

Chambon, J., Le Magueresse, T., Minck, O., and Antoni, J. (**2020**). "3D Beamforming for wind tunnel applications using ESM based transfer functions," Berlin Beamforming Conference .

Chardon, G. (**2022**). "Theoretical analysis of beamforming steering vector formulations for acoustic source localization," Journal of Sound and Vibration **517**, doi: 10.1016/j.jsv.2021.116544.

Curle, N. (**1955**). "The influence of solid boundaries upon aerodynamic sound," Proceedings of the Royal Society of London. Series A, Mathematical and Physical Sciences **231**(1187), 505–514.

Dunn, M. H., and Tinetti, A. F. (**2004**). "Aeroacoustic scattering via the equivalent source method," AIAA Aerospace Sciences Meeting **10**.

Evans, D., Hartmann, M., and Delfs, J. (**2019**). "Beamforming for point force surface sources in numerical data," Journal of Sound and Vibration **458**, 303–319, doi: 10.1016/j.jsv.2019.05.030.

Ewert, R., and Schröder, W. (**2003**). "Acoustic perturbation equations based on flow decomposition via source filtering," J. Comput. Phys. **188**(2), 365–398, doi: 10.1016/S0021-9991(03)00168-2.

Ffowcs Williams, J. E., and Hawkings, D. L. (**1969**). "Sound generation by turbulence and surfaces in arbitrary motion," Philosophical Transactions of the Royal Society of London. Series A, Mathematical and Physical Sciences **264**, 321 – 342.

Gao, J., Wu, H., and Jiang, W. (**2020**). "Dipole-based beamforming method for locating dipole sources with unknown orientations in three-dimensional domains," Journal of the Acoustical Society of America **147**(1), 125–136, doi: 10.1121/10.0000491.

Holland, K. R., and Nelson, P. A. (**2012**). "An experimental comparison of the focused beamformer and the inverse method for the characterisation of acoustic sources in ideal and non ideal acoustic environments," Journal of Sound and Vibration **331**, 4425–4437, doi: https://doi.org/10.1016/j.jsv.2012.05.005.

Jordan, P., Fitzpatrick, J., and Valiere, J.-C. (**2002**). "Measurement of an aeroacoustic dipole using a linear microphone array," Journal of the Acoustical Society of America **111**, 1267–73, doi: 10.1121/1.1446052.

Koopmann, G. H., Song, L., and Fahnline, J. B. (**1989**). "A method for computing acoustic fields based on the principle of wave superposition," Journal of the Acoustical Society of America **86**, 2433–2438, doi: 10.1121/1.404042.

Le Magueresse, T. (**2016**). "Approche unifiée multidimensionelle du problème d'identification acoustique inverse," Ph.D. thesis, LAUM & LVA.

Le Magueresse, T., Outrequin, A., Thivant, M., Antoni, J., and Jouvray, J.-L. (**2020**). "3D acoustical characterization of an electrical engine by Bayesian focusing," 8th Berlin Beamforming Conference https://www.bebec.eu/fileadmin/bebec/downloads/bebec-2020/papers/BeBeC-2020-D19.pdf.

Leclère, Q., Aujogue, N., Dinsenmeyer, A., Antoni, J., and Julliard, E. (**2020**). "Characterization of engine jet noise in flight conditions using advanced acoustic imaging methods," in *Berlin Beamforming Conference*.

Leclère, Q., Pereira, A., Bailly, C., Antoni, J., and Picard, C. (**2017**). "A unified formalism for acoustic imaging based on microphone array measurements," International Journal of Aeroacoustics **16**, 431–456, doi: 10.1177/1475472X17718883.

Lee, S. (**2017**). "Review: The use of Equivalent Source Method in computational acoustics," Journal of Computational Acoustics **25**(01), doi: 10.1142/S0218396X16300012.

Lighthill, M. J. (**1952**). "On sound generated aerodynamically. I. General theory," Proceedings of the Royal Society of London. Series A, Mathematical and Physical Sciences **211**(1107), 564–587.

Liu, Y., Quayle, A., Dowling, A., and Sijtsma, P. (**2008**). "Beamforming correction for dipole measurement using two-dimensional microphone arrays," Journal of the Acoustical Society of America **124**, 182–91, doi: 10.1121/1.2931950.

Merino-Martinez, R., Sijtsma, P., M.Snellen *et al.* (**2019**). "A review of acoustic imaging methods using phased microphone arrays," CEAS Aeronautical Journal **10**, 197–230, doi: 10.1007/s13272-019-00383-4.

Najafi-Yazdi, A., Brès, G., and Mongeau, L. (**2011**). "An acoustic analogy formulation for moving sources in uniformly moving media," Proceedings of The Royal Society A Mathematical Physical and Engineering Sciences **467**, 144–165, doi: 10.1098/rspa.2010.0172.

Norton, M. P., and Karczub, D. G. (**2003**). *Fundamentals of Noise and Vibration Analysis for Engineers*, 2 ed. (Cambridge University Press).

Pan, S., Yang, J., Kaiqiang, W., Wang, Z., and Deng (**2020**). "Study on radiated noise of a panel under fluctuating surface pressure due to an Idealized Side Mirror," Applied Sciences **10**, 994, doi: 10.3390/app10030994.

Porteous, R., Prime, Z., Doolan, C., Moreau, D., and Valeau, V. (**2015**). "Three-dimensional beamforming of dipolar aeroacoustic sources," Journal of Sound and Vibration **355**, doi: 10.1016/j.jsv.2015.06.030.

Sarradj, E. (**2012**). "Three-dimensional acoustic source mapping with different beamforming steering vector formulations," Advances in Acoustics and Vibration **2012**, doi: 10.1155/2012/292695.

Siemens (**Siemens 2021**). "Simcenter STAR-CCM+, version 2021.1" .

Wang, Y., Gu, Z., Li, W., and Lin, X. (**2010**). "Evaluation of aerodynamic noise generation by a generic side mirror," **37**, doi: 10.5281/zenodo.1071039.